Essential role of limiting telomeres in the pathogenesis of Werner syndrome

Sandy Chang[1], Asha S Multani[1], Noelia G Cabrera[1], Maria L Naylor[2], Purnima Laud[1], David Lombard[3], Sen Pathak[1], Leonard Guarente[4] & Ronald A DePinho[2]

Mutational inactivation of the gene *WRN* causes Werner syndrome, an autosomal recessive disease characterized by premature aging, elevated genomic instability and increased cancer incidence[1,2]. The capacity of enforced telomerase expression to rescue premature senescence of cultured cells from individuals with Werner syndrome[3] and the lack of a disease phenotype in Wrn-deficient mice with long telomeres[4] implicate telomere attrition in the pathogenesis of Werner syndrome. Here, we show that the varied and complex cellular phenotypes of Werner syndrome are precipitated by exhaustion of telomere reserves in mice. In late-generation mice null with respect to both *Wrn* and *Terc* (encoding the telomerase RNA component), telomere dysfunction elicits a classical Werner-like premature aging syndrome typified by premature death, hair graying, alopecia, osteoporosis, type II diabetes and cataracts. This mouse model also showed accelerated replicative senescence and accumulation of DNA-damage foci in cultured cells, as well as increased chromosomal instability and cancer, particularly nonepithelial malignancies typical of Werner syndrome. These genetic data indicate that the delayed manifestation of the complex pleiotropic of Wrn deficiency relates to telomere shortening.
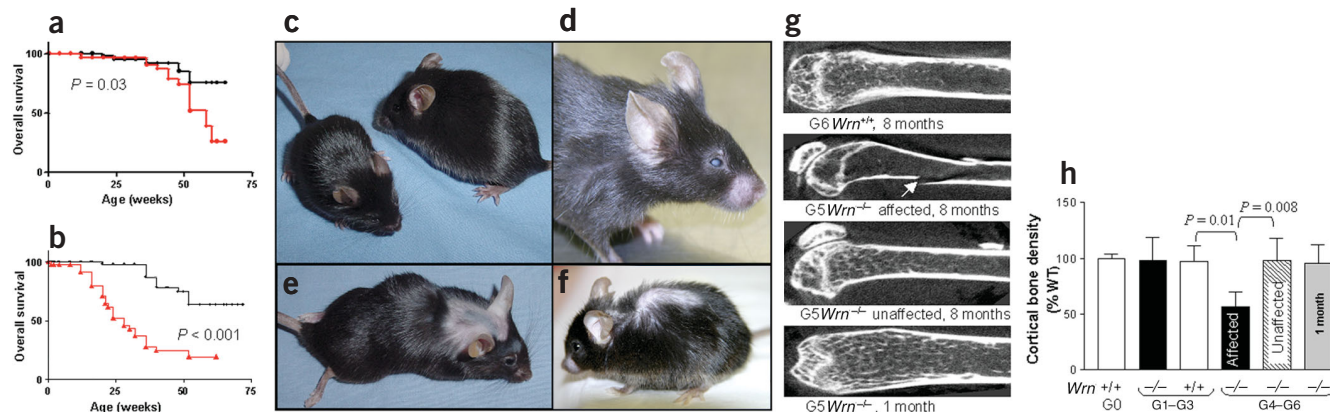

Figure 1 Reduced lifespan and premature aging phenotypes in G4–G6 *Terc*$^{-/-}$ *Wrn*$^{-/-}$ mice. (**a**) Kaplan-Meier analysis of overall survival of G1–G3 *Terc*$^{-/-}$ *Wrn*$^{-/-}$ (n = 42; red line) and *Terc*$^{-/-}$ *Wrn*$^{+/+}$ (n = 55; black line) mice. (**b**) Kaplan-Meier analysis of overall survival of G4–G6 *Terc*$^{-/-}$ *Wrn*$^{-/-}$ (n = 39; red line) and *Terc*$^{-/-}$ *Wrn*$^{+/+}$ (n = 47; black line) mice. (**c**) 4-week-old female G5 *Terc*$^{-/-}$ *Wrn*$^{-/-}$ mouse (left) and age-matched female G5 *Terc*$^{-/-}$ *Wrn*$^{+/+}$ littermate control (right). (**d**) 3-month-old G5 *Terc*$^{-/-}$ *Wrn*$^{-/-}$ mouse with cataract in right eye. (**e**) 8-week-old G5 *Terc*$^{-/-}$ *Wrn*$^{-/-}$ mouse with alopecia. (**f**) 12-week-old G6 *Terc*$^{-/-}$ *Wrn*$^{-/-}$ mouse with kyphosis. (**g**) Micro-computed tomography imaging of femurs of a 32-week-old G6 *Terc*$^{-/-}$ *Wrn*$^{+/+}$ mouse, a 32-week-old affected G5 *Terc*$^{-/-}$ *Wrn*$^{-/-}$ mouse with Werner syndrome, a 32-week-old unaffected G5 *Terc*$^{-/-}$ *Wrn*$^{-/-}$ mouse and a 4-week-old G5 *Terc*$^{-/-}$ *Wrn*$^{-/-}$ mouse. The arrow indicates a pathological fracture. (**h**) Cortical bone density in femurs (n = 4–6) from 8-month-old G0 *Terc*$^{-/-}$ *Wrn*$^{+/-}$, G1–G3 *Terc*$^{-/-}$ *Wrn*$^{-/-}$, G4–G6 *Terc*$^{-/-}$ *Wrn*$^{+/+}$, affected G4–G6 *Terc*$^{-/-}$ *Wrn*$^{-/-}$, unaffected G4–G6 *Terc*$^{-/-}$ *Wrn*$^{-/-}$ and 4-week-old G5 *Terc*$^{-/-}$ *Wrn*$^{-/-}$ mice. Bone density data are indicated as a percentage of G0 *Terc*$^{-/-}$ *Wrn*$^{+/-}$ control femurs with error bars representing s.e.m.

[1]Department of Molecular Genetics, M.D. Anderson Cancer Center, Box 11, 1515 Holcombe Blvd., Houston, Texas 77030, USA. [2]Department of Medical Oncology, Dana-Farber Cancer Institute; Departments of Medicine and Genetics, Harvard Medical School, 44 Binney Street (M413), Boston, Massachusetts 02115, USA. [3]Department of Pathology, Brigham and Women's Hospital, Boston, Massachusetts 02115, USA. [4]Department of Biology, Massachusetts Institute of Technology, Cambridge, Massachusetts 02139, USA. Correspondence should be addressed to S.C. (schang@mdanderson.org) or R.A.D. (ron_depinho@ dfci.harvard.edu).

Table 1 Age-related changes in late-generation telomerase-Werner compound mutant mice

Genotype	G0 $Wrn^{+/+}$	G4–G6 $Wrn^{+/+}$	Affected G4–G6 $Wrn^{-/-}$	Unaffected G4–G6 $Wrn^{-/-}$
Number of mice examined for pathologies	48	47	39	23
Maximum lifespan	114 weeks	92 weeks	30.5 weeks	89 weeks
Minimum lifespan	24 weeks	24 weeks	3 weeks	31 weeks
Median lifespan	94 weeks	78 weeks	24 weeks	69 weeks
Body weight	10% reduction at 18 months	16% reduction at 18 months	20% reduction at birth, 30% reduction at 8 months	Reduction at 8 months
Lordokyphosis	Moderate at 18 months	Severe at 18 months	Normal at 1 month, severe by 8 months	Severe at 18 months
Osteoperosis	Not observed	Not observed	Normal at 1 month, 11 of 11 by 4–8 months	Not observed
Cataract formation	Not observed	Not observed	None at 1 month, 8 of 39 by 4–8 months	Not observed
Glucose tolerance	Normal	Normal	Normal at 1 month, 10 of 12 glucose intolerant by 4 months	Normal
Insulin resistance	Normal	Normal	Normal at 1 month, 3 of 3 insulin resistant by 4 months	Normal
Hair graying	3 of 48 by 18 months	11 of 47 by 18 months	Normal at 1 month, 19 of 39 by 8 months	7 of 23 by 18 months
Hair regrowth	12% reduction at 18 months	32% reduction by 18 months	Normal at 1 month, 61% reduction by 4 months	ND
Alopecia	2 of 48 by 18 months	14 of 47 by 18 months	Normal at 1 month, 23 of 39 by 8 months	8 of 23 by 18 months
Wound healing	ND	Healed by day 14	Healed by day 20	ND
Peripheral WBC, RBC	Normal	Normal	Normal	Normal
CBC	Normal	Normal	Normal	Normal
Subcutaneous adipose	5% reduction at 18 months	17% reduction at 18 months	43% reduction at 4 months	20% reduction at 18 months
Muscle mass	10% reduction at 18 months	21% reduction at 18 months	13% reduced at 8 months	ND
Gonad mass	Normal at 18 months	13% reduction at 18 months	69% reduction at 4 months	5% reduction at 8 months
Spleen mass	Normal at 18 months	19% reduction at 18 months	11% reduction at 8 months	22% reduction at 18 months
Atherosclerosis	Normal at 18 months	Normal at 18 months	Normal at 8 months	Normal at 18 months

Mice (at least four per time point) were assessed for aging phenotypes at 1, 4, 8 and 18 months of age. All aging comparisons were made against age-matched G0 $Wrn^{+/+}$ controls. Tissue samples were stained with hematoxylin and eosin and assessed microscopically. Physiological testing for cognitive and cardiovascular functions was not done. WBC, white blood cells; RBC, red blood cells; CBC, complete blood count; ND, not determined.

Individuals with Werner syndrome develop a spectrum of age-related disorders and have a greater risk for nonepithelial cancers[5,6]. *WRN* encodes a RecQ DNA helicase[7] involved in DNA recombination, replication and repair[8–10]. The hyper-recombination and multiple chromosomal aberrations in cells from individuals with Werner syndrome[11–13] support the hypothesis that accelerated aging and increased cancer susceptibility stem from the failure to suppress illegitimate recombination events and global genome instability[2]. Fibroblasts from individuals with Werner syndrome have accelerated telomere attrition and undergo premature senescence that can be rescued by enforced expression of Tert[3,14]. These cell culture–based observations, coupled with the fact that *Wrn* knockout mice have long telomeres but are essentially normal[4,15], fueled speculation that telomere attrition is a key element in the pathogenesis of Werner syndrome. Apart from the cellular impact of telomere dysfunction in Werner syndrome, we speculate that the impaired activity of DNA repair in the setting of telomere dysfunction[16,17] could exacerbate the DNA structural defects brought about by Wrn deficiency.

To address this hypothesis, we carried the *Wrn* null allele through successive generational intercrosses with $Terc^{-/-}$ mice to produce $Terc^{-/-} Wrn^{+/+}$ and $Terc^{-/-} Wrn^{-/-}$ cohorts with progressively shorter telomeres and increasing telomere dysfunction. In first and second generation (G1 and G2) $Terc^{-/-}$ mice, *Wrn* status had no discernable impact on clinical appearance, weight gain or lifespan (median lifespan 92 ± 3.1 weeks for G1–G2 $Terc^{-/-} Wrn^{+/+}$ mice versus 89 ± 4.5

weeks for G1–G2 $Terc^{-/-} Wrn^{-/-}$ mice; $P = 0.21$; **Fig. 1a** and **Supplementary Table 1** online). In sharp contrast, G4–G6 $Terc^{-/-} Wrn^{-/-}$ mice had lower body weights (20% reduction at 4 weeks of age and 30% reduction at 32 weeks of age; $P = 0.01$) than $Terc^{-/-} Wrn^{+/+}$ mice and shorter median survival times (24 ± 5.6 weeks for G4–G6 $Terc^{-/-} Wrn^{-/-}$ mice and 78 ± 9.2 weeks for G4–G6 $Terc^{-/-} Wrn^{+/+}$ mice; $P < 0.001$; **Fig. 1b** and **Table 1**). All cohorts appeared to be healthy through early adulthood, but a substantial proportion of 12- to 16-week-old G4–G6 $Terc^{-/-} Wrn^{-/-}$ mice (~63% of the cohort: 25 of 36 females and 14 of 26 males) had clinical features of premature aging, typical of Werner syndrome, including hair loss, cataract formation and severe hypogonadism (**Fig. 1c–f, Table 1** and **Supplementary Fig. 1** online). We surmised that this variable penetrance could relate to the heterogeneity of telomere reserves in a given $Terc^{-/-}$ generation. Finally, the progressive nature of the premature aging phenotypes in successive $Terc^{-/-}$ generations was also evident as a function of advancing age; several 72-week-old G3 $Terc^{-/-} Wrn^{-/-}$ mice, which were normal through young and middle adulthood, experienced accelerated aging relative to age-matched G3 $Terc^{-/-} Wrn^{+/+}$ controls (**Supplementary Table 1** online and data not shown). The latter observations establish an age-progressive aspect to Werner syndrome in mice, as is seen in humans.

A substantial proportion of G4–G6 $Terc^{-/-} Wrn^{-/-}$ mice also had other Werner syndrome phenotypes, including early-onset osteoporosis, type II diabetes, cataract formation and impaired wound healing
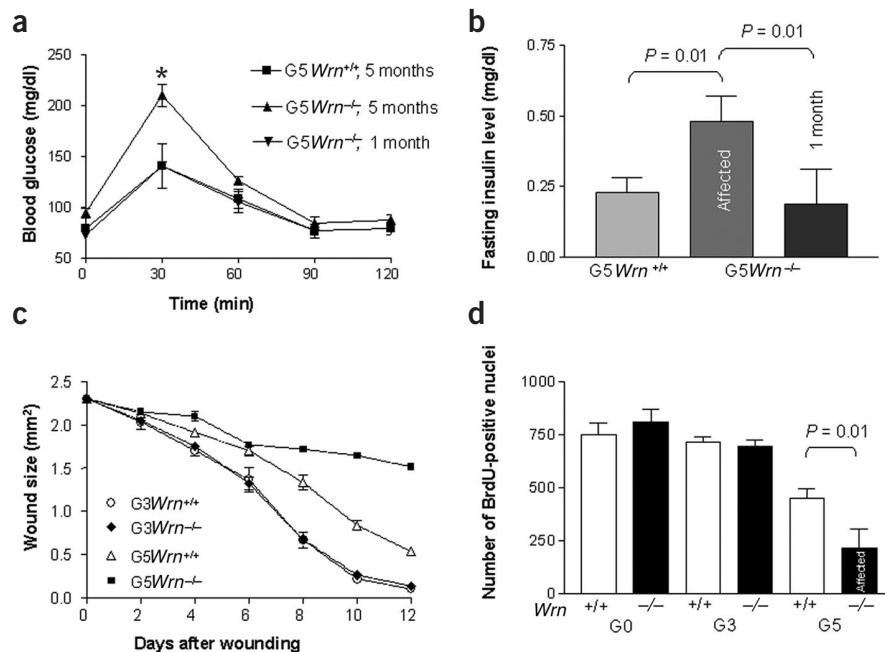
Figure 2 Glucose intolerance and wound healing defects in G5 *Terc*^{−/−} *Wrn*^{−/−} mice. (**a**) Mice fasted for 15 h, and 2 g D-glucose per kg body weight was injected intraperitoneally. Blood glucose concentrations were sampled from tail bleeds at the indicated times from 4-week-old G5 *Terc*^{−/−} *Wrn*^{−/−} female mice (*n* = 3), 20-week-old G5 *Terc*^{−/−} *Wrn*^{−/−} mice with Werner syndrome (*n* = 12, 7 females, 5 males) and 20-week-old G5 *Terc*^{−/−} *Wrn*^{+/+} controls (*n* = 10, 5 males, 5 females). Values are the mean ± s.e.m. *P = 0.01 30 min after glucose administration (Student's *t*-test). (**b**) Fasting serum insulin levels in 4- and 16-week-old G5 *Terc*^{−/−} *Wrn*^{−/−} female mice (*n* = 3 each) and G5 *Terc*^{−/−} *Wrn*^{+/+} female controls (*n* = 3). Blood samples were collected and serum was analyzed by ELISA. (**c**) Wound healing assay. Wound diameters were measured with a caliper in G3 *Terc*^{−/−} *Wrn*^{+/+} and *Terc*^{−/−} *Wrn*^{−/−} mice (*n* = 4 each) and in G5 *Terc*^{−/−} *Wrn*^{+/+} and *Terc*^{−/−} *Wrn*^{−/−} mice (*n* = 8 each). Values represent the mean ± s.e.m. at each time point. (**d**) Number of cells positive for 5-bromodeoxyuridine (BrdU) observed at wound edges in 24-week-old mice of the indicated genotypes. G0 mice are *Terc*^{+/−}; G1–G6 mice are *Terc*^{−/−}.

(**Table 1**). By 32 weeks of age, all G4–G6 *Terc*^{−/−} *Wrn*^{−/−} mice showing outward signs of premature aging also had hunched spines (kyphosis), femoral bones with decreased cortical thickness and trabecular mass by micro-computed tomography and histological morphometric analyses (**Fig. 1f–h** and data not shown), and radiographic pathological fractures (**Fig. 1g**). Skeletal integrity and normal bone density were maintained in age-matched G4–G6 *Terc*^{−/−} *Wrn*^{+/+} and G1–G3 *Terc*^{−/−} *Wrn*^{−/−} controls and in 4-week-old G4–G6 *Terc*^{−/−} *Wrn*^{−/−} mice, underscoring the age-progressive nature of the skeletal phenotype. Ten of 12 prematurely aged 20-week-old G4–G6 *Terc*^{−/−} mice were also diagnosed with type II diabetes, on the basis of elevated fasting blood glucose levels, abnormal glucose tolerance tests and increased endogenous insulin levels, the latter consistent with a compensatory hyperinsulinemia due to decreased insulin responsiveness of peripheral tissues, as observed in human type II diabetes (**Fig. 2a,b**). All glucose and insulin measurements were normal in 4-week-old G4–G6 *Terc*^{−/−} *Wrn*^{−/−} mice and in 20-week-old G4–G6 *Terc*^{−/−} *Wrn*^{+/+} and G1 *Terc*^{−/−} *Wrn*^{−/−} controls (**Fig. 2a,b** and data not shown). Finally, consistent with the chronic skin ulcerations that afflict individuals with Werner syndrome, 24-week-old prematurely aged G5 *Terc*^{−/−} *Wrn*^{−/−} mice suffered from impaired healing of acute wounds (**Fig. 2c**); they had delayed wound closure (20 d versus 14 d in *Terc*^{−/−} *Wrn*^{+/+} mice; data not shown) and fewer cells that were positive for 5-bromodeoxyuridine at the sites of wound re-epithelialization (**Fig. 2d**).

To reinforce a link between the onset of premature-aging phenotypes in Werner syndrome and telomere dysfunction, we examined gastrointestinal crypts and primary bone marrow cells for the presence of telomere dysfunction. Gastrointestinal crypt epithelium provides a quantitative *in situ* system in which to gauge the degree of telomere dysfunction as a function of successive *Terc*^{−/−} generations and advancing age[18] (**Fig. 3**). Late-generation *Terc*^{−/−} *Wrn*^{−/−} mice had a marked increase in intestinal crypt cell apoptosis relative to age- and generation-matched *Terc*^{−/−} *Wrn*^{+/+} controls (**Fig. 3b**). Serial analysis showed that intestinal crypt cell apoptotic bodies were infrequent between 5 and 12 weeks of age but became abundant by 20 weeks of age (**Fig. 3c**); this rise in apoptosis paralleled the increased anaphase

bridge index (**Fig. 3d**). Late-generation *Terc*^{−/−} *Wrn*^{−/−} mice showing no signs of premature aging by 8 months of age also had reduced levels of apoptosis and anaphase bridging relative to prematurely aged *Terc*^{−/−} *Wrn*^{−/−} mice of the same age and cohort (**Fig. 3b,d**). Mirroring these gastrointestinal crypt data, all of nine primary bone marrow metaphases derived from prematurely aged G4–G6 *Terc*^{−/−} *Wrn*^{−/−} mice had more p-p arm fused chromosomes (a hallmark of telomere dysfunction; **Fig. 4a** and **Supplementary Table 2** online) and more telomere signal-free ends (**Fig. 4b**, P = 0.005), as well as accelerated loss in overall telomere lengths by quantitative fluorescence *in situ* hybridization (FISH) analysis (**Fig. 4c**; P < 0.001 relative to age-matched G1 and G3 *Terc*^{−/−} *Wrn*^{−/−} mice and P = 0.01 relative to G4–G6 *Terc*^{−/−} *Wrn*^{+/+} controls). Correspondingly, G4–G6 *Terc*^{−/−} *Wrn*^{−/−} mice showing no outward signs of premature aging had fewer signal-free ends (**Fig. 4b**) and greater average telomere length (**Fig. 4b,c**) relative to prematurely aged G4–G6 *Terc*^{−/−} *Wrn*^{−/−} mice. G4–G6 *Terc*^{−/−} *Wrn*^{−/−} mice with the earliest onset of premature aging phenotypes had shorter telomeres (**Supplementary Table 2** online and data not shown), further supporting the idea that telomere shortening drives Werner syndrome pathogenesis.

Werner syndrome is associated with elevated genomic instability and increased cancer incidence, particularly of osteosarcomas and soft tissue sarcomas[6,12,13]. Bone marrow metaphases derived from prematurely aged G4–G6 *Terc*^{−/−} *Wrn*^{−/−} mice showed marked genomic instability, manifesting as more chromosomal p-p, p-q and q-q arm fusions than in early-generation and G5 *Terc*^{−/−} *Wrn*^{+/+} controls (**Fig. 4d** and **Supplementary Table 2** online). Spectral karyotyping analysis detected multiple nonreciprocal translocations involving several chromosomes (**Fig. 4e** and **Supplementary Fig. 2** online). Although prematurely aged G4–G6 *Terc*^{−/−} *Wrn*^{−/−} mice were not prominently cancer-prone (presumably related to premature death), G1–G3 *Terc*^{−/−} *Wrn*^{−/−} mice routinely succumbed to osteosarcomas and soft tissue sarcomas with a median latency of 63 weeks (**Fig. 4f** and **Supplementary Table 3** online). This contrasts with the later onset (85 weeks) and lymphoma preponderance in G1–G3 *Terc*^{−/−} *Wrn*^{+/+} mice (**Fig. 4f** and **Supplementary Table 3**
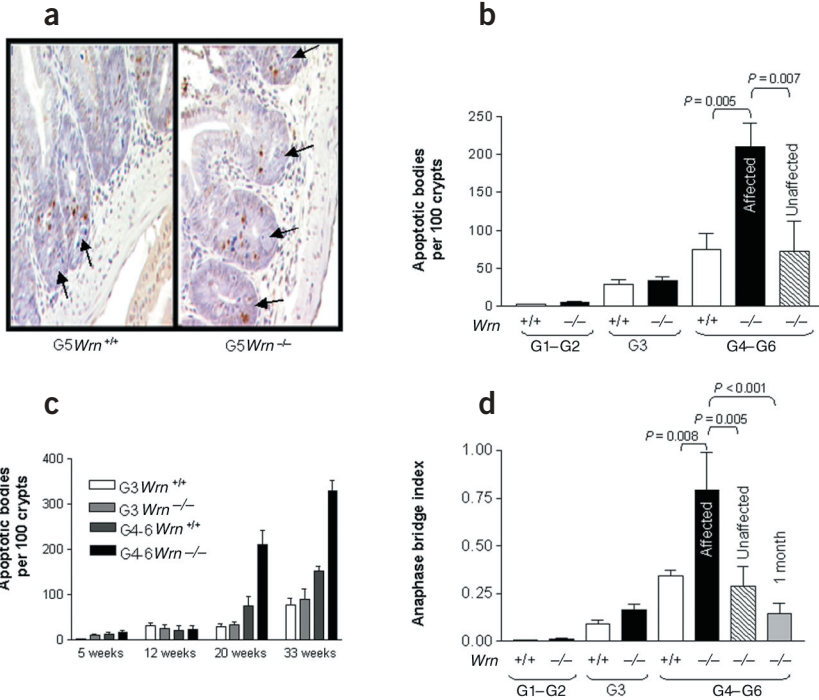
Figure 3 Increased apoptosis and anaphase bridges in gastrointestinal crypts of G4–G6 Terc^{−/−} Wrn^{−/−} mice. (**a**) TUNEL-positive apoptotic bodies in G5 Terc^{−/−} Wrn^{+/+} and Terc^{−/−} Wrn^{−/−} intestinal crypts. Arrows indicate intestinal crypts containing apoptotic nuclei. (**b**) Number of apoptotic bodies in hematoxylin and eosin–stained sections of intestinal crypts of 20-week-old G1–G2 Terc^{−/−} Wrn^{−/−} and Terc^{−/−} Wrn^{+/+}, G3 Terc^{−/−} Wrn^{−/−} and Terc^{−/−} Wrn^{+/+}, and G4–G6 Terc^{−/−} Wrn^{−/−} and Terc^{−/−} Wrn^{+/+} mice (n = 3–5 per genotype). Hatched bar shows data from unaffected G4–G6 Terc^{−/−} Wrn^{−/−} mice. (**c**) Number of apoptotic cells in intestinal crypts from mice of the indicated genotypes at various ages (n = 3 per group). G0 mice are Terc^{+/−}; G1–G6 mice are Terc^{−/−}. (**d**) Percentage of intestinal crypts from 20-week-old mice of the indicated genotypes containing at least one anaphase bridge. G0 mice are Terc^{+/−}; G1–G6 mice are Terc^{−/−}

online). On the cellular level, cultured fibroblasts from individuals with Werner syndrome had decreased replicative potential and abnormal cytogenetic profiles[12–14]. Correspond-ingly, 3T3 assays documented a profound reduction of replicative potential lifespan (**Fig. 5a**) and increased chromosomal structural aberrations in G5 Terc^{−/−} Wrn^{−/−} mouse embryonic fibroblasts (MEFs) compared with

G5 Terc^{−/−} Wrn^{+/+} controls (**Supplementary Fig. 3** online). Replicative senescence in human fibroblasts may be mediated by a telomere-dependent DNA-damage checkpoint response, manifesting as an accumulation of 53BP1 and γH2AX nuclear foci[19,20]. Correspondingly, >95% of passage 2 G5 Terc^{−/−} Wrn^{−/−} MEFs had prominent nuclear 53BP1 and γH2AX foci, compared with <5% of

Figure 4 Accelerated telomere loss results in increased genomic instability and enhanced tumor predisposition in affected G4–G6 Terc^{−/−} Wrn^{−/−} mice. (**a**) Bone marrow metaphases isolated from 23-week-old G5 Terc^{−/−} Wrn^{+/+} and Wrn^{−/−} mice were collected for metaphase spreads (n = 9 each); telomeres were labeled by PNA-FISH (red) and chromosomes by DAPI (blue). Arrows indicate fused chromosomes. (**b**) Quantification of telomere signal-free chromosome ends from bone marrow metaphase spreads from mice of the indicated genotypes. G0 mice are Terc^{+/−}; G1–G6 mice are Terc^{−/−}. Hatched bar shows data from unaffected G4–G6 Terc^{−/−} Wrn^{−/−} mice (n = 3). (**c**) Quantitative PNA-FISH of bone marrow metaphases isolated directly from 22- to 25-week-old mice of the indicated genotypes. G0 mice are Terc^{+/−}; G1–G6 mice are Terc^{−/−}. Hatched bar shows data from unaffected G4–G6 Terc^{−/−} Wrn^{−/−} mice (n = 3). (**d**) Chromosome aberrations in bone marrow metaphases of 22- to 25-week-old mice of the indicated genotypes. G0 mice are Terc^{+/−}; G1–G6 mice are Terc^{−/−}. (**e**) Representative spectral karyotyping (SKY) and DAPI labeling of splenocyte metaphases derived from 16-week-old G5 Terc^{−/−} Wrn^{−/−} mice (n = 3). Nonreciprocal translocations involving chromosome 3, 4, 10, 11 and X are indicated. DC, dicentric; Frag, chromosome fragment. (**f**) Kaplan-Meier curves of tumor-free survival of G1–G3 Terc^{−/−} Wrn^{−/−} mice (n = 25; red line) versus Terc^{−/−} Wrn^{+/+} littermates (n = 31; black line). Table shows tumor distribution (Lymp, lymphoma; Sarc, sarcoma; Osteo, osteosarcoma; Carc, carcinoma). Actual tumor numbers are indicated above, and percentage of total below.
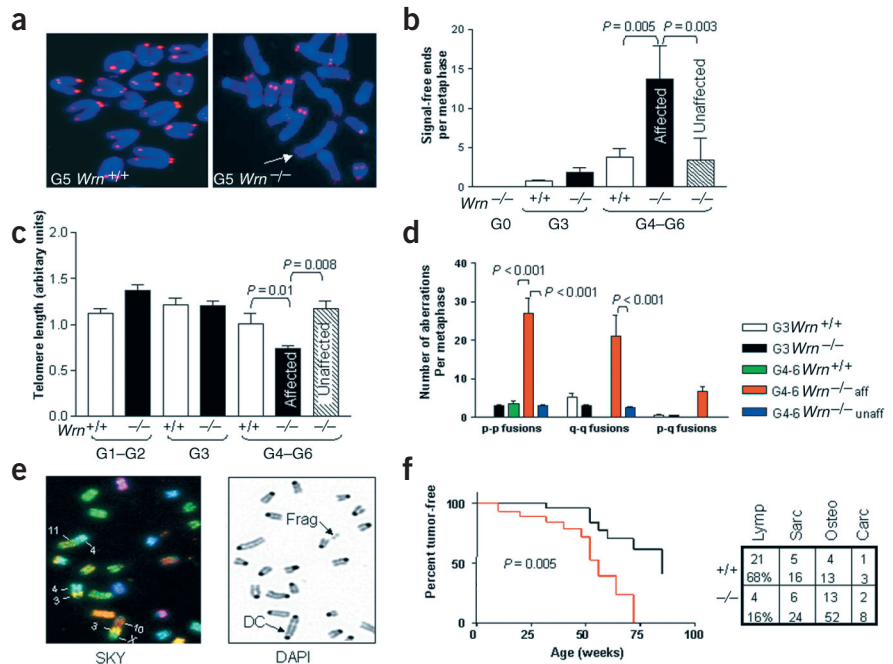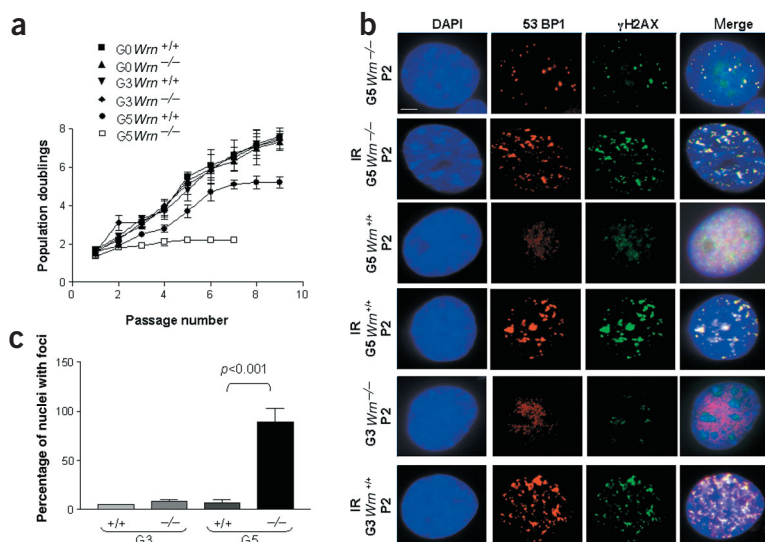
Figure 5 Premature replicative senescence and increased DNA damage response in G4–G6 *Terc*−/− *Wrn*−/− cells. (**a**) Growth properties of *Terc*+/− *Wrn*+/+ (*n* = 5), *Terc*+/− *Wrn*−/− (*n* = 3), G3 *Terc*−/− *Wrn*+/+ (*n* = 4), G3 *Terc*−/− *Wrn*−/− (*n* = 4), G5 *Terc*−/− *Wrn*+/+ (*n* = 8) and G5 *Terc*−/− *Wrn*−/− (*n* = 7) MEFs passaged on a 3T3 protocol. (**b**) 53BP1 (red) and γH2AX (green) immunostaining in passage 2 MEFs of the indicated genotypes. G0 mice are *Terc*+/−; G1–G6 mice are *Terc*−/−. IR indicates MEFs that were treated with 5 Gy of γ-irradiation and then subjected to immunofluorescence analysis after 30 min. Scale bar, 0.5 μm. (**c**) Quantification of 53BP1- and γH2AX-positive foci in passage 2 MEFs of the indicated genotypes (all MEFs were *Terc*−/−). G0 mice are *Terc*+/−; G1–G6 mice are *Terc*−/−.

passage 2 G5 *Terc*−/− *Wrn*+/+ and G3 *Terc*−/− *Wrn*−/− MEFs (**Fig. 5b,c**). Consistent with the established role of these foci in the DNA-damage response, MEFs of all three genotypes readily formed 53BP1 and γH2AX foci after 5 Gy of γ-irradiation (**Fig. 5b**). These results suggest that, in the presence of telomere dysfunction, Wrn deficiency is associated with increased DNA-damage signals. These findings are consistent with the cytogenetic documentation of eroded telomeres and interstial chromosomal breaks in metaphase spread of late-generation *Terc*−/− *Wrn*−/− cells.

In this study, we found that late-generation *Terc*−/− *Wrn*−/− mice recapitulate most of the classical clinical features of Werner syndrome, establishing these compound mutant mice as a model for human Werner syndrome. The premature aging phenotypes (such as osteoporosis, cataracts and diabetes) seen in late-generation *Terc*−/− *Wrn*−/− mice were not observed in age-matched late-generation *Terc*−/− *Wrn*+/+ controls, supporting the idea that telomere dysfunction in the setting of Wrn deficiency unmasks additional phenotypes characteristic of those observed in individuals with Werner syndrome. Unlike late-generation *Terc*−/− mice that have degenerative phenotypes in highly proliferative compartments (intestine, skin and blood)[21], late-generation *Terc*−/− *Wrn*−/− mice are predominantly affected in the mesenchymal tissues. These findings suggest that the modest impact of WRN deficiency in human epithelial compartments could relate to tissue stem cell telomerase activity or, more likely, the presence of functional redundancy among the ReqQ helicase family, particularly the BLM helicase[22]. Our data are consistent with the emerging view that WRN is involved in telomere dynamics, as evidenced by the capacity of WRN to interact with the telomere-binding protein TRF2 (ref. 23) and affect the 3′ single strand telomeric overhang[24]. Wrn deficiency may precipitate telomere uncapping at a longer set length and further exacerbate telomere dysfunction, providing a basis for aging phenotypes that target slowly proliferating mesenchymal tissues. This mouse model thus provides a molecular entry point for studying the complex interactions of Wrn deficiency and telomere dysfunction in generating genomic instability, premature aging and cancer.

METHODS

Production of *Terc*−/− *Wrn*−/− mice. To reduce the number of generations required to achieve critical telomere shortening, we crossed *Terc*+/+ *Wrn*−/− mice and G3 *Terc*−/− *Wrn*+/+ mice to generate our starting generation (G0) *Terc*+/− *Wrn*+/− mice. G3 *Terc*−/− mice show no evidence of telomere dysfunction, indicating that they have ample telomere reserve at the time of this initial cross[21].

We intercrossed G0 *Terc*+/− *Wrn*+/− mice in a cousin-mating scheme to generate G1 *Terc*−/− *Wrn*+/+, *Wrn*+/− and *Wrn*−/− mice. We intercrossed G1 *Terc*−/− *Wrn*+/− mice to produce G2 mice and so on, until G6 mice were produced. The mixed genetic background of our cohorts was 55% C57BL6, 37.5% 129Sv, 6.25% BALB/c and 1.25% SLJ[16,18,21]. The M. D. Anderson Cancer Center Institutional Animal Care and Use Committee approved all mouse experiments.

Mouse growth and analysis of aging phenotypes. We weighed mice from the indicated cohorts weekly until 1 year of age, examined them closely for signs of malnutrition and ill health and killed them if they were profoundly ill. We scored all deaths by Kaplan-Meier analysis and measured statistical significance using the log-rank test. We carried out comprehensive gross and autopsy analysis on all killed mice. We collected organs, fixed them in 10% formalin, embedded them in paraffin and stained 10-μm sections with hematoxylin and eosin.

Alopecia and wound-healing analysis. We obtained skin biopsy samples from different parts of the mouse's body, embedded them in paraffin and stained cross-sections with hematoxylin and eosin. We quantified hair loss by counting the number of hair shafts in each sample and normalizing the counts to those of samples from age-matched *Terc*+/− *Wrn*+/+ mice. We assessed wound healing ability in mouse cohorts by carrying out 3-mm-punch, full-thickness biopsies through the epidermis and dermis to the panniculus carnosus using a dermal skin punch. We measured wound sizes at 0, 4, 6, 8, 10 and 12 d after wounding.

Bone density determination. We stripped the left leg of each mouse to be analyzed free of skeletal muscle and fixed it in 70% ethanol for 1 week. We then placed it into a GE micro-computed tomography scanner and scanned it at 4.5T for 1.5 h, achieving a resolution of 20 μm. We analyzed the resulting image with the Bone Morphometric software and determined cortical and trabecular bone mass. We then decalcified the same bone, sectioned it with a diamond knife and stained it with hematoxylin and eosin. We determined cortical and trabecular bone thickness by morphometry.

Glucose tolerance tests and serum insulin analysis. We injected glucose (2 mg per g body weight) intraperitoneally into mice 16 h after fasting. We collected blood from tail veins 0, 0.5, 1, 2 and 4 h after injection and analyzed it with a home glucose analyzer (Elite). We collected serum samples from fasting mice and analyzed them for insulin levels by ELISA (Linco Labs).

Intestinal apoptosis and anaphase bridge index. We stained formalin-fixed intestinal sections for TUNEL activity using the apoptotag kit (Intergen), following the manufacturer's protocols. We quantified anaphase bridges directly from intestinal sections stained with hematoxylin and eosin and scored them as described[17]. We measured statistical significance using the log-rank test.

Tumor incidence. We monitored mice daily for evidence of tumor growth and killed them if tumors exceeded 1.5 cm. We processed tumors for histological analysis as described above. We calculated tumor incidence by Kaplan Meier analysis.

Cytogenetics, quantitative telomere FISH and spectral karyotyping analysis. We prepared metaphase chromosomes from bone marrow cells or splenocytes 1 h after intraperitoneal injection of colcemid (2 mg per kg body weight). This direct chromosome collection eliminated any possibility that the observed chromosomal aberrations were due to culturing artifacts. We prepared metaphases from MEFs as described[21]. We subjected metaphases to Giemsa staining or quantitative FISH analysis of telomeric sequences with Cy-3-labeled T_2AG_3 peptide-nucleic acid (PNA) probe. We carried out spectral karyotyping analysis according to the manufacturer's recommendations, using mouse chromosome paint probes (Applied Spectral Imaging) on a Nikon Eclipse 800 microscope equipped with an ASI interferometer and workstation. Depending on the quality of metaphase spreads, 10–20 metaphases from each sample were analyzed in detail.

Cell cultures and 3T3 assay. We prepared MEFs from individual G0, G3 and G5 $Terc^{-/-} Wrn^{-/-}$, $Terc^{-/-} Wrn^{+/-}$ and $Terc^{-/-} Wrn^{+/+}$ embryos at embryonic day 13.5. We used at least four independently derived MEF cell lines of each genotype in all analyses. We carried out serial passages of cell lines according to the NIH3T3 protocol.

Immunofluorescence microscopy. We fixed MEFs with 2% paraformaldehyde for 10 min and permeabilized them with 0.5% Triton X-100 for 10 min. We used rabbit antibody to human 53BP1 and mouse antibody to human γH2AX (Upstate Biotechnology) at 1:500 dilution. We used Alexa 488– and Alexa 595–conjugated secondary antibodies (Molecular Probes) at 1:1,000. Only nuclei with four or more foci were scored as positive for telomere dysfunction[20], and at least 250 nuclei were scored per genotype.

Note: Supplementary information is available on the Nature Genetics website.

Published online at http://www.nature.com/naturegenetics/

1. Martin, G.M. & Oshima, J. Lessons from human progeroid syndromes. *Nature* **408**, 263–266 (2000).
2. Hickson, I.D. RecQ helicases: caretakers of the genome. *Nat. Rev. Cancer* **3**, 169–178 (2003).
3. Wyllie, F.S. *et al.* Telomerase prevents the accelerated cell ageing of Werner syndrome fibroblasts. *Nat. Genet.* **24**, 16–17 (2000).
4. Lombard, D.B. *et al.* Mutations in the WRN gene in mice accelerate mortality in a p53-null background. *Mol. Cell. Biol.* **9**, 3286–3291 (2000).
5. Epstein, C.J., Martin, G.M., Schultz, A. & Motulsky, A.G. Werner's syndrome: a review of its symptomatology, natural history, pathologic features, genetics and relationship to the natural aging process. *Medicine* **45**, 5893–5897 (1966).
6. Goto, M., Miller, R.W., Ishikawa, Y. & Sugano, H. Excess of rare cancers in Werner syndrome (adult progeria). *Cancer Epidemiol. Bio. Prev.* **5**, 239–246 (1996).
7. Yu, C.E. *et al.* Positional cloning of the Werner's syndrome gene. *Science* **272**, 258–262 (1996).
8. Suzuki, N. *et al.* DNA helicase activity in Werner's syndrome gene product synthesized in a baculovirus system. *Nucleic Acids Res.* **25**, 2973–2978 (1997).
9. Watt, P.M., Louis, E.J., Borts, R.H. & Hickson, I.D. Sgs1: a eukaryotic homolog of E. coli RecQ that interacts with topoisomerase II *in vivo* and is required for faithful chromosome segregation. *Cell* **81**, 253–260 (1995).
10. Yan, H., Chen, C.Y., Kobayashi, R. & Newport, J. Replication focus-forming activity 1 and the Werner syndrome gene product. *Nat. Genet.* **19**, 375–378 (1998).
11. Myung, K., Datta, A., Chen, C. & Kolodner, R.D. SGS1, the Saccharomyces cerevisiae homologue of BLM and WRN, suppresses genome instability and homeologous recombination. *Nat. Genet.* **27**, 113–116 (2001).
12. Salk, D., Au, K., Hoehn, H. & Martin, G.M. Cytogenetics of Werner's syndrome cultured skin fibroblasts: variegated translocation mosaicism. *Cytogenet. Cell Genet.* **30**, 92–107 (1981).
13. Melcher, R. *et al.* Spectral karyotyping of Werner syndrome fibroblast cultures. *Cytogenet. Cell Genet.* **91**,180–185 (2000).
14. Schulz, V.P. *et al.* Accelerated loss of telomeric repeats may not explain accelerated replicative decline of Werner syndrome cells. *Hum. Genet.* **97**, 750–754 (1996).
15. Lebel, M. & Leder, P. A deletion within the murine Werner syndrome helicase induces sensitivity to inhibitors of topoisomerase and loss of cellular proliferative capacity. *Proc. Natl. Acad. Sci. USA* **95**, 13097–13102 (1998).
16. Wong, K.K. *et al.* Telomere dysfunction impairs DNA repair and enhances sensitivity to ionizing radiation. *Nat. Genet.* **26**, 85–88 (2000).
17. Goytisolo, F.A. *et al.* Short telomeres result in organismal hypersensitivity to ionizing radiation in mammals. *J. Exp. Med.* **192**, 1625–1636 (2000).
18. Wong, K.K. *et al.* Telomere dysfunction and ATM deficiency compromises organ homeostasis and accelerates ageing. *Nature* **421**, 643–648 (2003).
19. d'Adda di Fagagna, F. *et al.* A DNA damage checkpoint response in telomere-initiated senescence. *Nature* **426**, 194–198 (2003).
20. Takai, H., Smogorzewska, A. & de Lange, T. DNA damage foci at dysfunctional telomeres. *Curr. Biol.* **13**, 1549–1556 (2003).
21. Rudolph, K.L. *et al.* Longevity, stress response, and cancer in aging telomerase-deficient mice. *Cell* **96**, 701–712 (1999).
22. Kaneko, H. *et al.* Expression of the BLM gene in human haematopoietic cells. *Clin. Exp. Immunol.* **118**, 285–289 (1999).
23. Opresko, P.L. *et al.* Telomere-binding protein TRF2 binds to and stimulates the Werner and Bloom syndrome helicases. *J. Biol. Chem.* **277**, 41110–41119 (2002).
24. Orren, D.K., Theodore, S. & Machwe, A. The Werner syndrome helicase/exonuclease (WRN) disrupts and degrades D-loops in vitro. *Biochemistry* **41**, 13483–13488 (2002).